ESC HEART FAILURE
ESC Heart Failure 2023; **10**: 2510–2523
Published online 8 June 2023 in Wiley Online Library (wileyonlinelibrary.com) **DOI:** 10.1002/ehf2.14404

ORIGINAL ARTICLE

Activating transcription factor 4 drives the progression of diabetic cardiac fibrosis

Yu Li[1], Qian He[1], Chao-Yong He[1], Chao Cai[1], Zhen Chen[1] and Jing-Zhu Duan[2]*

[1]*Department of Cardiology, Shiyan Taihe Hospital (Hubei University of Medicine), Shiyan, China; and* [2]*Department of Respiratory, Shiyan Taihe Hospital (Hubei University of Medicine), Shiyan, China*

Abstract

Aims Diabetic cardiomyopathy (DC) is one of serious complications of diabetic patients. This study investigated the biological function of activating transcription factor 4 (ATF4) in DC.

Methods and results Streptozotocin-treated mice and high glucose (HG)-exposed HL-1 cells were used as the *in vivo* and *in vitro* models of DC. Myocardial infarction (MI) was induced by left coronary artery ligation in mice. Cardiac functional parameters were detected by echocardiography. Target molecule expression was determined by real time quantitative PCR and western blotting. Cardiac fibrosis was observed by haematoxylin and eosin and Masson's staining. Cardiac apoptosis was evaluated by terminal deoxynucleotidyl transferase dUTP nick end labelling. Activities of superoxide dismutase, glutathione peroxidase, and levels of malonic dialdehyde and reactive oxygen species were used to assess oxidative stress damage. Molecular mechanisms were evaluated by chromatin immunoprecipitation, dual luciferase assay, and co-immunoprecipitation. ATF4 was up-regulated in the DC and MI mice ($P < 0.01$). Down-regulation of ATF4 improved cardiac function as evidenced by changes in cardiac functional parameters ($P < 0.01$), inhibited myocardial collagen I ($P < 0.001$) and collagen III ($P < 0.001$) expression, apoptosis ($P < 0.001$), and oxidative stress ($P < 0.001$) in diabetic mice. Collagen I ($P < 0.01$) and collagen III ($P < 0.01$) expression was increased in MI mice, which was reversed by ATF4 silencing ($P < 0.05$). ATF4 depletion enhanced viability ($P < 0.01$), repressed apoptosis ($P < 0.001$), oxidative damage ($P < 0.001$), and collagen I ($P < 0.001$), and collagen III ($P < 0.001$) expression of HG-stimulated HL-1 cells. ATF4 transcriptionally activated Smad ubiquitin regulatory factor 2 (Smurf2, $P < 0.001$) to promote ubiquitination and degradation of homeodomain interacting protein kinase-2 ($P < 0.001$) and subsequently caused inactivation of nuclear factor erythroid 2-related factor 2/heme oxygenase 1 pathway ($P < 0.001$). The inhibitory effects of ATF4 silencing on HG-induced apoptosis ($P < 0.01$), oxidative injury ($P < 0.01$), collagen I ($P < 0.001$), and collagen III ($P < 0.001$) expression were reversed by Smurf2 overexpression.

Conclusions ATF4 facilitates diabetic cardiac fibrosis and oxidative stress by promoting Smurf2-mediated ubiquitination and degradation of homeodomain interacting protein kinase-2 and then inactivation of nuclear factor erythroid 2-related factor 2/heme oxygenase 1 pathway, suggesting ATF4 as a treatment target for DC.

Keywords ATF4; Diabetic cardiomyopathy; Fibrosis; HIPK2; Oxidative stress; Smurf2

Received: 13 October 2022; Revised: 10 March 2023; Accepted: 2 May 2023
**Correspondence to: Jing-Zhu Duan, Department of Respiratory, Shiyan Taihe Hospital (Hubei University of Medicine), No. 32, Renmin South Road, Shiyan 442000, Hubei Province, China. Email: duanzhujingg542@163.com*

Introduction

Diabetes remains a serious public health issue due to its increasing prevalence worldwide. Diabetic cardiomyopathy (DC), a diabetes-associated complication characterized by diastolic dysfunction and cardiac fibrosis, may lead to heart failure.[1] It has been recognized that cardiac fibrosis is enhanced during DC development.[2] Myocardial fibrosis under high glucose condition is triggered by the imbalance of matrix protein synthesis and degradation, and subsequent extracellular matrix deposition, which eventually results in cardiac structure changes and function impairment.[3] Therefore,

better understanding the molecular mechanisms and developing interventions for cardiac fibrosis can effectively delay the progression of DC.

Activating transcription factor 4 (ATF4) belongs to cAMP-response element binding protein (CREB)/ATF family, which can serve as either an activator or a repressor of gene transcription.[4] As a transcriptional factor, ATF4 is responsible for the regulation of endoplasmic reticulum stress.[5] ATF4 functions as a modulator of the cellular hypoxic response and contributes to the activation of genes that maintain normal endoplasmic reticulum function and facilitate survival.[6] ATF4 is involved in various pathophysiological processes, such as apoptosis, metabolism, antioxidant defence, tumourigenesis, and so on.[7] A recent study reported the physiological role of ATF4 in insulin secretion in response to glucose stimulation.[8] Importantly, ATF4 was down-regulated in high glucose-stimulated H9c2 cells and diabetic rat hearts.[9] Another study reported that ATF4 contributed to renal tubulointerstitial fibrosis in mice with diabetic nephropathy.[10] So far, the regulatory roles of ATF4 in diabetic cardiac fibrosis have not been elucidated.

Smad ubiquitin regulatory factor 2 (Smurf2) is an E3 ubiquitin ligase that participates in the regulation of protein homeostasis.[11] A recent study demonstrated that deletion of Smad3 attenuated cardiac fibrosis via inhibition of Smurf2-mediated ubiquitin and degradation of Smad7.[12] Besides, Smurf2 was demonstrated to be up-regulated in the *in vitro* model of diabetic cardiac fibrosis.[13] Interestingly, ATF4 was predicted to bind to Smurf2 promoter by bioinformatics analysis.

Nuclear factor erythroid 2-related factor 2 (Nrf2)/heme oxygenase 1 (HO-1) pathway is a crucial protective mechanism by which confers protection against oxidative stress injury. Extensive evidence has indicated that activation of Nrf2/HO-1 pathway is responsible for remission of DC.[14,15] Li et al. documented that Nrf2/HO-1 pathway activation ameliorated myocardial fibrosis under diabetic condition.[16] However, the up-stream regulatory mechanisms of Nrf2/HO-1 pathway in diabetic cardiac fibrosis are poorly understood. Homeodomain interacting protein kinase-2 (HIPK2), belonged to the HIPK family, takes part in multiple biological processes, such as proliferation, inflammation, and autophagy.[17–19] Notably, HIPK2 was reported to alleviate hypoxia/reoxygenation-induced myocardial injury via enhancing Nrf2 transcription.[20] So far, the involvement of HIPK2/Nrf2 axis in diabetic cardiac fibrosis has not been documented. By bioinformatics analysis, we found that Smurf2 was predicted to promote the ubiquitination and degradation of HIPK2.

Based on the above background, we hypothesized that high expression of ATF4 might transcriptionally activate Smurf2 to cause ubiquitination and degradation of HIPK2, and subsequently inactivate Nrf2/HO-1 pathway, which finally promoted high glucose-induced cardiac fibrosis. Our study for the first time uncovered the biological function of ATF4 and its underlying mechanisms in diabetic cardiac fibrosis, suggesting ATF4 as a potential therapeutic target to prevent diabetic cardiac fibrosis progression.

Methods

Animal procedure

Male C57BL/6 mice weighed 20 ± 2 g were obtained from Slac Jingda Laboratory Animal Co., Ltd. (Hunan, China) and randomly divided into normal, DC, DC + shNC, and DC + shATF4 groups (n = 5 per group). The animal experiments were approved by the ethical committee of Shiyan Taihe Hospital (Hubei University of Medicine) (approval number: 202061). Diabetics were induced by intraperitoneal injection of 50 mg/kg streptozotocin (STZ) for five consecutive days, whereas citrate buffer in equal volume was injected into the non-diabetes control mice. One week later, fasting blood glucose was measured. The mice with fasting blood glucose of more than 16.7 mmol/L were regarded as diabetics. A myocardial injection with lentiviruses carrying shATF4 or negative control shRNA (shNC) (1×10^7 UT/30 μL, GenePharma, Shanghai, China) was carried out after the final STZ injection for 12 weeks. Twelve weeks after lentivirus injection, the body weight, fasting blood glucose concentration, and fasting blood insulin level were detected. Then, all mice were euthanized, and the hearts were collected and weighed.

Myocardial infarction (MI) was induced in male C57BL/6 mice (weighing 20 ± 2 g, 8 weeks old), as described previously.[21] There were four experimental groups: sham, MI, MI + shNC, and MI + shATF4 (n = 5 per group). Briefly, mice were anaesthetized using intraperitoneal injection with pentobarbital sodium (50 mg/kg). A left-sided thoracotomy was performed to expose the heart. The anterior descending branch of the left coronary artery was ligated. Successful ligation of the artery was confirmed by tissue blanching. For sham mice, the suture was passed beneath the coronary artery and not tied. The chest was closed and the mice were allowed to recover. The lentiviruses carrying shATF4 or shNC (1×10^7 UT/30 μL) was injected into the left ventricular cavity with the aorta artery cross-clamped before ligation of left descending coronary artery. The mice were euthanized by cervical dislocation at 4 weeks after MI.

Echocardiographic evaluation

The M-mode echocardiography was adopted for echocardiographic evaluation using the Vevo2100 animal echocardiography machine (Visual Sonics, Toronto, Canada). After anesthetization with 1.5% isoflurane, the mice were fixed and the left ventricular end-systolic diameter, left ventricular end-diastolic dimension, left ventricular end-systolic volume, left ventricular end-diastolic volume, left ventricular posterior

wall thickness, left ventricular anterior wall thickness, left ventricular ejection fraction (LVEF), and left ventricular fractional shortening (LVFS) were measured using Vevo2100 Imaging System, and data were analysed using VisualSonics VevoLab software.

Histological analysis

The hearts of mice were fixed in 4% paraformaldehyde for 24 h at 4°C, followed by dehydration, paraffin embedding, and cutting into 5-μm sections. The pathological changes were analysed by standard haematoxylin and eosin (H&E) staining using the H&E Staining Kit (catalogue number: SL7070, Coolaber, Beijing, China). Cardiac fibrosis was determined using the Masson Staining Kit (catalogue number: SL7230, Coolaber). The stained sections were photographed under a light microscope.

Terminal deoxynucleotidyl transferase dUTP nick end labelling

Apoptosis in heart tissues was determined using the terminal deoxynucleotidyl transferase dUTP nick end labelling assay kit (catalogue number: ab206386, Abcam, Cambridge, UK). The paraffin-embedded sections of heart tissues were deparaffinized, followed by exposure to proteinase K for rupture of the cell membrane at room temperature for 20 min and treatment with 3% H_2O_2 at room temperature for 5 min, and then incubated with TdT labelling reaction mix for 1.5 h at 37°C. After developing with diaminobenzidine (DAB) solution for 15 min at room temperature, the sections were viewed under the microscope (Olympus, Japan). The apoptotic rate of the brains was calculated.

Cell culture and treatment

HL-1 mouse cardiomyocytes (catalogue number: SCC065, Sigma-Aldrich, St. Louis, USA) were maintained in DMEM (Thermo Fisher, Waltham, USA) containing 10% FBS (Gibco, New York, USA) at 37°C with 5% CO_2. To simulate diabetes *in vitro*, HL-1 cells were exposed to 30 mM glucose (HG) for 48 h. The control cells were cultured in 5.5 mM glucose (normal glucose, NG) supplemented with 24.5 mM mannitol for the condition of being homotonic (HO).

Cell transfection

Short hairpin RNA (shRNA) targeting ATF4 (shATF4, 2 μg), 2 μg Smurf2 (shSmurf2, 2 μg), and negative control shRNA (shNC, 2 μg), HIPK2 overexpression plasmid (oeHIPK2, 2 μg), 2 μg oeSmurf2 and 2 μg vector were provided by GenePharma (Shanghai, China) and transfected into HL-1 cells using Lipofectamine 3000 (Thermo Fisher) for 24 h at 37°C following the directions of the manufacturer.

Real time quantitative polymerase chain reaction

Total RNA was isolated using TRIzol reagent (catalogue number: 15596026, Thermo Fisher). First-strand cDNA was generated from 2 μg RNA using the Super Script VILO kit (catalogue number: 11754050, Thermo Fisher). qPCR was carried out using the iQ SYBR® Green Supermix (catalogue number: #1708887, Bio-Rad, Hercules, USA). The thermocycling conditions were initial denaturation at 95°C for 5 min; 38 cycles of denaturation at 95°C for 10 s, annealing at 60°C for 20 s and extension at 72°C for 30 s. Gene expression levels were analysed using the $2^{-\Delta\Delta CT}$ method. Primers for qPCR are listed in *Table S1*. Three independent experiments were conducted.

Western blotting

RIPA lysis buffer (catalogue number: P0013C, Beyotime, Haimen, China) was adopted for total protein extraction from mouse hearts or HL-1 cells. For isolation of nuclear protein, the Nucleoprotein Extraction Kit (catalogue number: C500009, Sangon Biotech, Shanghai, China) was used. After protein concentration quantification, protein samples with equal amount (50 μg) were separated by sodium dodecyl sulfate polyacrylamide gel electrophoresis (SDS-PAGE), transferred onto polyvinylidene difluoride (PVDF) membranes, and blocked in 5% skim milk for 1 h at room temperature. The membranes were probed with primary antibodies against ATF4 (bs-1531R, 1:500, Bioss, Beijing, China), collagen I (bs-0578R, 1:500, Bioss), collagen III (bs-0549R, 1:500, Bioss), HIPK2 (bs-6353R, 1:500, Bioss), Nrf2 (bs-1074R,1:100, Bioss), HO-1 (BM4010, 1:500, BOSTER, Wuhan, China), Smurf2 (#12024, 1:1000, Cell Signaling Technology, Trask Lane Danvers, USA), histone H3 (A12477-2, 1:500, BOSTER), and β-actin (BA2305, 1:2000, BOSTER) at 4°C overnight. Subsequently, the secondary antibody (#7074, 1:3000, Cell Signaling Technology) was applied for 1 h at room temperature. The immune blots were developed using the enhanced chemiluminescence (Millipore, USA) and subjected to densitometry analysis using ImageJ software (Bethesda, USA). Three independent experiments were conducted.

Cell viability evaluation

HL-1 cells were seeded into 96-well plates and subjected to various treatments. Then, cells were reacted with 0.5 mg/mL MTT solution (catalogue number: C0009S, Beyotime) for 4 h at 37°C. The supernatant was discarded and 100 μL DMSO was added to each well, followed by shaking at low speed for

10 min. Absorbance values were obtained at 570 nm on a microplate reader (Tecan, Switzerland). Three independent experiments were conducted.

Apoptosis detection

To determine cell apoptosis, the Annexin V-FITC/PI apoptosis detection kit (catalogue number: E-CK-A211, Elabscience, Wuhan, China) was used following the instructions. Briefly, 1×10^5 HL-1 cells were acquired and subjected to successive staining with 2.5 μL of Annexin V-FITC and 2.5 μL PI solution for 15 min in a dark place. Finally, the apoptotic cells were analysed on a flow cytometer (Partec, Goerlitz, Germany). Three independent experiments were conducted.

Reactive oxygen species measurement

The intracellular reactive oxygen species (ROS) was detected using two kinds of probes, including dihydroethidium (DHE, red fluorescence) and 2',7'-Dichlorodihydrofluorescein diacetate (DCFH-DA, green fluorescence). The ROS production in heart tissues was evaluated by DHE staining. The heart sections were incubated with 10 μM DHE (catalogue number: S0063, Beyotime) at 37°C for 30 min. The nuclei were stained with DAPI. The ROS level in HL-1 cells was detected by DCFH-DA probe (catalogue number: S0033S, Beyotime). Cells were stained with 10 μM DCFH-DA at 37°C for 20 min. The fluorescence was observed under a fluorescence microscope. Three independent experiments were conducted.

Determination of superoxide dismutase, glutathione peroxidase, and malonic dialdehyde

The activities of superoxide dismutase (SOD), glutathione peroxidase (GSH-Px), and malonic dialdehyde (MDA) concentration in heart tissues and cells were assessed using the total superoxide dismutase assay kit (catalogue number: S0109, Beyotime), total glutathione peroxidase assay kit (catalogue number: S0059S, Beyotime) and lipid peroxidation MDA assay kit (catalogue number: S0131S, Beyotime) according to the manufacturer's protocols. Three independent experiments were conducted.

Dual-luciferase reporter assay

The wild type (WT) Smurf2 promoter sequences or the mutant (MUT) sequences were amplified and inserted into the pGL3 luciferase reporter vector. Cells (5×10^5) were seeded in 24-well plates and transfected with either pGL3-basic or the established promoter WT and MUT luciferase reporter plasmids together with vector or oeATF4 plasmid using Lipofectamine 3000 at 37°C. Luciferase activity was measured at 48 h after transfection using a Dual-Luciferase Reporter Assay System (catalogue number: RG027, Beyotime). Three independent experiments were conducted.

Chromatin immunoprecipitation

Chromatin immunoprecipitation (ChIP) assay was performed to determine the binding between ATF4 and Smurf2 promoter using the Pierce Agarose ChIP Kit (catalogue number: 26156, Thermo Fisher). In brief, cells were treated with 1% formaldehyde for 10 min at room temperature, and chromatin fragments were produced by ultrasound using a 10 s on and 10 s off mode for 12 cycles at 4°C. Immunoprecipitation was executed using 2 μg of anti-Smurf2 antibody (#12024, Cell Signaling Technology) or anti-IgG NC antibody (#3900, Cell Signaling Technology) for 2 h at 4°C. The enrichment of ATF4 in the purified DNA was assessed by qPCR. Three independent experiments were conducted.

Co-immunoprecipitation

HEK293T cells were transfected with FLAG-labelled Smurf2, Myc-labelled HIPK2, HA-labelled Ubiquitination using Lipofectamine 3,000, followed by lysing in lysis buffer. M2 magnetic beads (catalogue number: A4596, Sigma-Aldrich) were adopted for immunoprecipitation at 4°C overnight. After washing for four times, the conjugated proteins were detected by western blotting with primary antibodies against Smurf2, HIPK2, Flag, Myc, and HA.

For another experiment, the HL-1 cell lysates (500 μg) were immunoprecipitated with anti-IgG (#3900, Cell Signaling Technology) or anti-Smurf2 (#12024, Cell Signaling Technology) and incubated with protein G-Agarose beads (Yeasen, Shanghai, China) at 4°C overnight. Subsequently, washing with 1 mL lysis buffer was performed for four times. Finally, the samples were subjected to western blotting. Three independent experiments were conducted.

Protein stability test

To assess protein stability, HL-1 cells were exposed to 20 μg/mL CHX (catalogue number: C112766, Aladdin, Shanghai, China) for 0, 15, 30, 60, 120, and 240 min at 37°C. The expression of target proteins was detected by western blotting. Three independent experiments were conducted.

Statistical analysis

All values are expressed as mean ± standard deviation (SD). Statistical analysis between two groups or among more than

Figure 1 ATF4 silencing improves cardiac function and relieves interstitial fibrosis in diabetic mice. (A, B) The mRNA and protein expression of ATF4 in heart tissues was determined by RT-qPCR and western blotting. LVEF (C) and LVFS (D) were detected by M-mode echocardiography. (E) Representative images of myocardial sections subjected to H&E staining and Masson's staining. (F) Apoptosis in cardiac tissues was evaluated by terminal deoxynucleotidyl transferase dUTP nick end labelling assay. (G) Western blotting analysis of collagen I and collagen III protein abundance in heart tissues. Data are presented as the mean ± SD (n = 5). $^{**}P < 0.01$, $^{***}P < 0.001$.

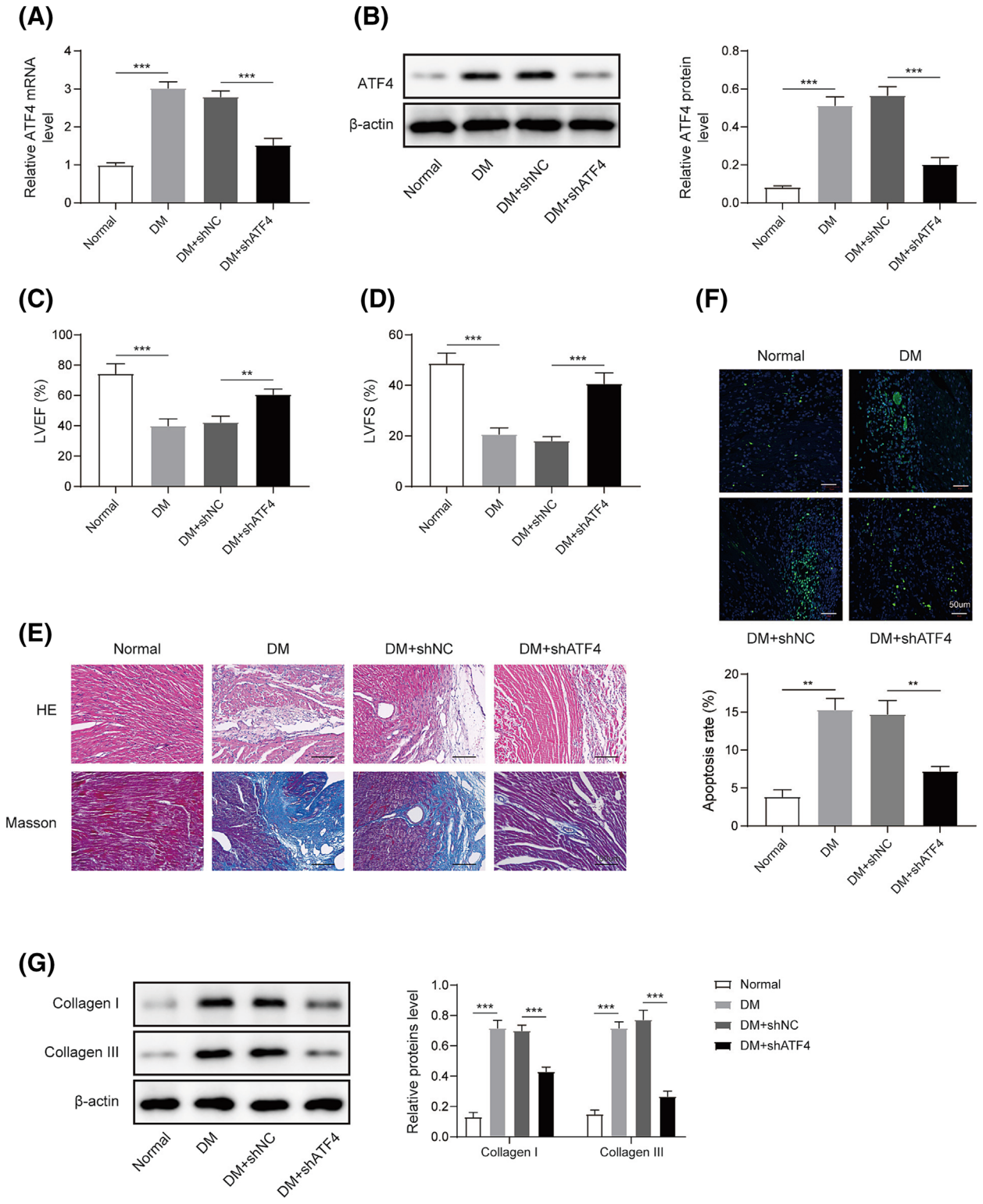

DOI: 10.1002/ehf2.14404

three groups was performed using Student's *t* test or one-way ANOVA followed by the Tukey's post hoc test using GraphPad prism 7. *P* values <0.05 were considered as statistically significant.

Results

Knockdown of activating transcription factor 4 attenuates diabetic cardiac fibrosis in mice

First, the expression of ATF4 in the heart tissues of diabetic mice was evaluated. Real time quantitative PCR (RT-qPCR) and western blotting results revealed that ATF4 level was strikingly enhanced in the diabetic group as compared with control group. However, administration with lentiviruses carrying shATF4 effectively reduced ATF4 level (*Figure 1A,B*). We observed an elevation in body weight, heart weight, fasting blood glucose concentration, and fasting blood insulin level in the diabetic group, which could be counteracted by ATF4 deficiency (*Figure S1A–D*). In addition, impaired cardiac function was found in STZ-induced diabetic mice as evidenced by reduction in diastolic and systolic left ventricular posterior wall thickness and left ventricular anterior wall thickness, and increase in left ventricular end-systolic diameter, left ventricular end-diastolic dimension, left ventricular end-systolic volume, left ventricular end-diastolic volume, LVEF, and LVFS, whereas silencing of ATF4 remarkably reversed the above changes of diabetic mice (*Figure 1C,D*; *Figure S1A–D*). Further H&E staining and Masson staining showed obvious pathological changes and collagen deposition in the hearts of STZ-treated mice; however, these changes could be counteracted by ATF4 knockdown (*Figure 1E*). Terminal deoxynucleotidyl transferase dUTP nick end labelling assay indicated that the apoptotic rate was elevated in the diabetic heart tissues, whereas ATF4 silencing reduced the apoptotic rate (*Figure 1F*). Besides, the protein levels of collagen I and collagen III were up-regulated in the heart tissues of diabetic mice, which were partly reversed by ATF4 depletion (*Figure 1G*). Furthermore, a mouse model of MI was established to evaluate the anti-fibrotic effects of ATF4 in the heart. We found that ATF4 was up-regulated in the heart of MI mice, which was silenced by injection with lentiviruses carrying sh-ATF4 (*Figure S2A*). Additionally, the enhanced expression of collagen I and collagen III in the heart tissues of MI mice was partly reversed by ATF4 knockdown (*Figure S2B*). These data proved that ATF4 depletion alleviated cardiac fibrosis of diabetic and MI mice.

Activating transcription factor 4 down-regulation restrains oxidative stress damage in hearts of diabetic mice

As oxidative stress is one of key characteristics of DC, we focused on the influence of ATF4 on cardiac oxidative stress damage of diabetic mice. As depicted in *Figure 2A–C*, there was a decrease in SOD and GSH-Px activities and increase in MDA level in the myocardial tissues of diabetic mice. Importantly, these changes were abrogated in diabetic mice after treatment with shATF4. Additionally, the production of ROS was enhanced in the diabetic mice, whereas the overproduction of ROS was attenuated by silencing of ATF4 (*Figure 2D*). Furthermore, western blotting was utilized to examine the expression of oxidative stress-related signal molecules. As compared with the normal mice, the expression of HIPK2, nuclear Nrf2, and HO-1 was distinctly declined in the diabetic group, which could be counteracted after ATF4 was knocked down (*Figure 2E*). Overall, inhibition of ATF4 relieved cardiac oxidative stress injury in diabetic mice.

Silencing of activating transcription factor 4 protects against high glucose-induced apoptosis, oxidative stress, and fibrosis in cardiomyocytes

To further validate the regulation of ATF4 in cardiac fibrosis *in vitro*, HL-1 cells were stimulated with HG to simulate hyperglycaemia. As presented in *Figure 3A*, HG exposure led to a remarkable elevation in ATF4 expression in HL-1 cells, while HO did not affect ATF4 expression. Subsequently, shATF4 was transfected into HL-1 cells, and the expression of ATF4 was significantly reduced (*Figure 3B*). Moreover, cell viability was evidently reduced after exposure to HG, whereas silencing of ATF4 raised the reduced viability of HL-1 cells (*Figure 3C*). ATF4 inhibition also repressed HG-triggered apoptosis of HL-1 cells (*Figure 3D*). In addition, the decreased SOD and GSH-Px activities and enhanced MDA and ROS levels in HG-challenged cells could be reversed by ATF4 knockdown (*Figure 3E–H*). Western blotting analysis revealed that collagen I, collagen III, and ATF4 were up-regulated, while HIPK2, nuclear Nrf2, and HO-1 were down-regulated by HG exposure. However, silencing of ATF4 effectively abolished HG-induced these changes (*Figure S3*). Therefore, consistent with the *in vivo* data, ATF4 inhibition restrained apoptosis, oxidative stress, and fibrosis in HG-stimulated HL-1 cells *in vitro*.

Overexpression of homeodomain interacting protein kinase-2 represses oxidative stress and fibrosis in high glucose-exposed cardiomyocytes via activation of nuclear factor erythroid 2-related factor 2/heme oxygenase 1 pathway

Next, we further explored the biological function of HIPK2 in HG-induced oxidative stress and fibrosis. To achieve this, oeHIPK2 was transfected into HL-1 cells to overexpress HIPK2 (*Figure 4*). RT-qPCR analysis indicated that the reduction of HIPK2 expression induced by HG was recovered by

Figure 2 ATF4 depletion suppresses oxidative stress in mice with diabetic cardiomyopathy. (A) SOD activity, (B) GSH-Px activity, (C) MDA level in heart tissues were assessed. (D) ROS production in hearts was evaluated by DHE staining. (E) Protein abundance of HIPK2, nuclear Nrf2 and HO-1 in myocardial tissues was assessed by western blotting. Data are presented as the mean ± SD (n = 5). $^{**}P < 0.01$, $^{***}P < 0.001$.

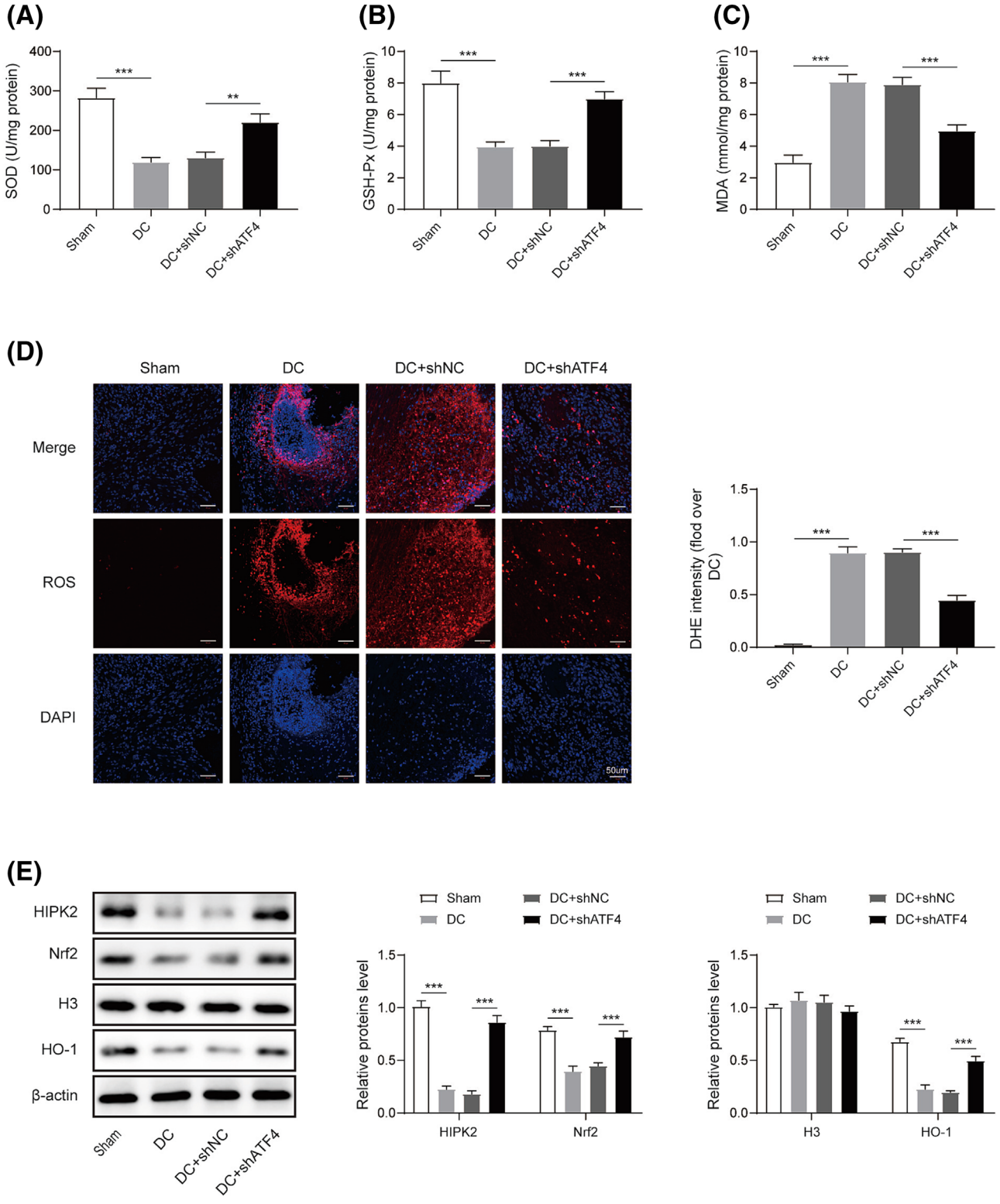

Figure 3 Inhibition of ATF4 attenuates apoptosis, oxidative stress, and fibrosis in HG-exposed cardiomyocytes. (A) ATF4 level in HL-1 cells after exposure to HG was determined by RT-qPCR. (B) The mRNA level of ATF4 in HL-1 cells transfected with sh-ATF4 was detected by RT-qPCR. (C) Cell viability was detected by MTT assay. (D) Flow cytometry analysis of cell apoptosis. (E) SOD activity, (F) GSH-Px activity, (G) MDA level in HL-1 cells were determined. (H) DCFH-DA staining for measurement of ROS release from HL-1 cells. Data are presented as the mean ± SD (n = 3). $^{**}P < 0.01$, $^{***}P < 0.001$.

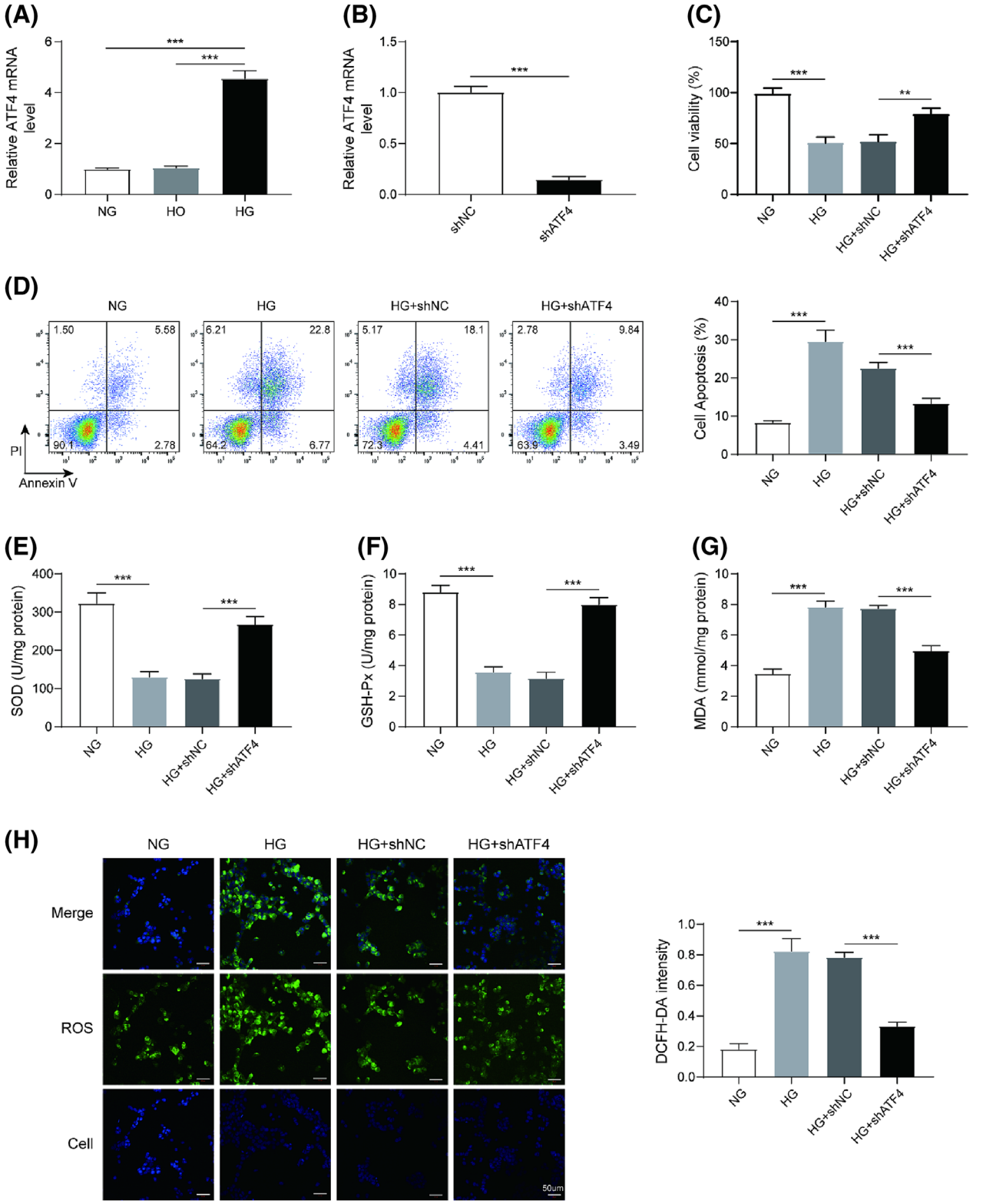

Figure 4 HIPK2 activates Nrf2/HO-1 pathway to alleviate oxidative stress and fibrosis in HG-exposed cardiomyocytes. (A, B) RT-qPCR analysis of HIPK2 mRNA expression in HL-1 cells with different treatments. (C) MTT assay for detection of cell viability. (D) Apoptotic rate of HL-1 cells was evaluated by flow cytometry. (E) SOD activity, (F) GSH-Px activity, (G) MDA level in HL-1 cells from various groups were detected. (H) Production of ROS from HL-1 cells was determined by DCFH-DA staining. Data are presented as the mean ± SD (n = 3). $^{**}P < 0.01$, $^{***}P < 0.001$.

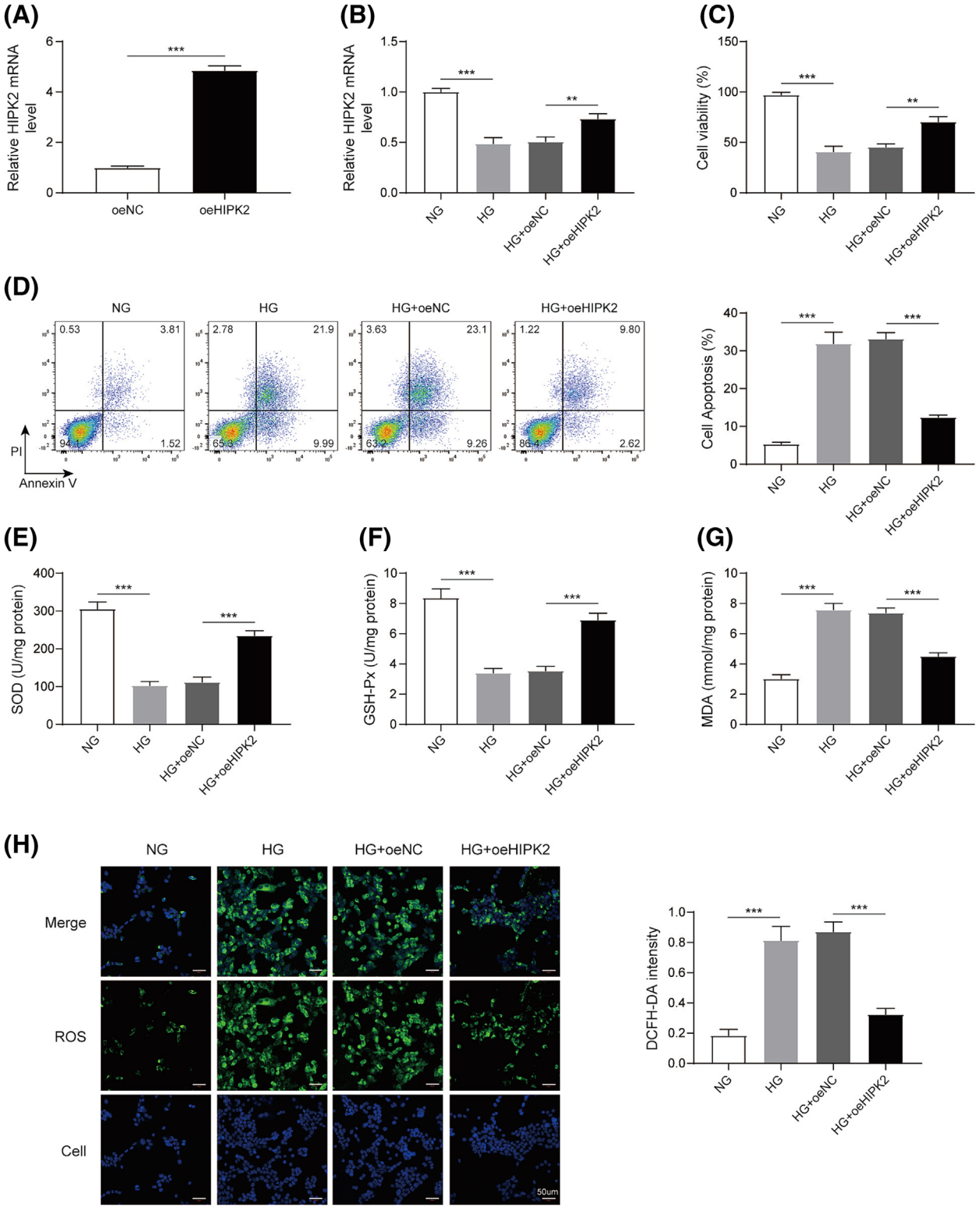

transfection with oeHIPK2 (*Figure 4*). In addition, overexpression of HIPK2 raised cell viability and reduced apoptotic rate of HG-stimulated HL-1 cells (*Figure 4C,D*). Furthermore, the decreased activities of SOD and GSH-Px, and elevated MDA level in response to HG could be reversed by enforced expression of HIPK2 (*Figure 4E–G*). DCFH-DA staining suggested that the excessive release of ROS triggered by HG could be restrained in HIPK2-overexpressed cells (*Figure 4H*). Besides, western blotting results showed that collagen I and collagen III levels were raised, while HIPK2, nuclear Nrf2, and HO-1 levels were decreased by HG stimulation; however, enforced expression of HIPK2 partially reversed these results (*Figure S4*). These observations demonstrated that HIPK2 overexpression inhibited HG-induced cardiac oxidative stress and fibrosis by activating Nrf2/HO-1 pathway.

Activating transcription factor 4 transcriptionally activates Smad ubiquitin regulatory factor 2 to promote ubiquitination and degradation of homeodomain interacting protein kinase-2

Next, we further investigated the molecular regulatory mechanism of ATF4 in HIPK2. We found that knockdown of ATF4 resulted in down-regulation of Smurf2 in HL-1 cells (*Figure 5A*). ChIP and dual-luciferase reporter assays confirmed that ATF4 could directly bind to the promoter of Smurf2 (*Figure 5B,C*). Moreover, transfection with shSmurf2 significantly inhibited the expression of Smurf2 (*Figure 5D*). More importantly, we found that exogenous and endogenous Smurf2 can directly bind to HIPK2 (*Figure 5E,F*). Silencing of Smurf2 significantly increased HIPK2 protein expression in HL-1 cells

Figure 5 ATF4 knockdown restrains Smurf2-mediated ubiquitination and degradation of HIPK2. (A) The mRNA level of Smurf2 after ATF4 silencing was assessed by RT-qPCR. (B) ChIP and (C) dual-luciferase reporter assays were carried out to determine the interaction between Smurf2 and ATF4. (D) Smurf2 mRNA expression after transfection with sh-Smurf2 was assessed by RT-qPCR. (E, F) The interplay between exogenous and endogenous Smurf2 and HIPK2 was validated by co-immunoprecipitation assay. (G) Protein abundance of HIPK2 in Smurf2-depleted HL-1 cells was detected by western blotting. (H) HIPK2 protein level in MG132-treated cells was determined by western blotting. Data are presented as the mean ± SD (n = 3). ***$P < 0.001$.

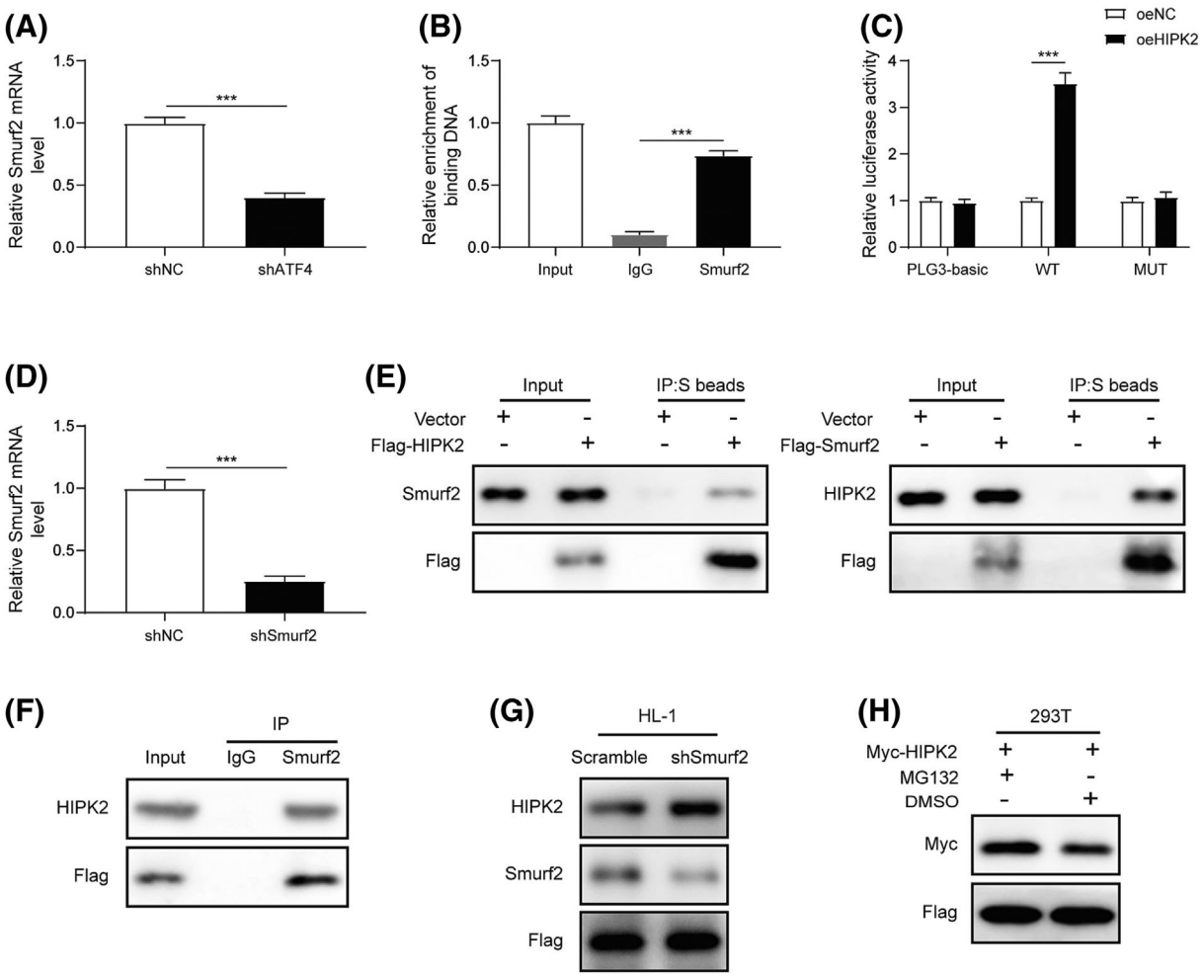

(*Figure 5G*). In addition, after treatment with MG132 (a potent proteasome inhibitor), the HIPK2 level was enhanced (*Figure 5H*). To determine HIPK2 protein stability, cells were exposed to CHX. As presented in *Figure 5J*, the exogenous HIPK2 protein was degraded in 293T cells with the extension of CHX treatment time, whereas MG132 could repress CHX-induced degradation of HIPK2 protein (*Figure S5A*). Besides, CHX-mediated endogenous HIPK2 protein degradation in HL-1 cells was restrained by Smurf2 depletion (*Figure S5B*). Co-immunoprecipitation assay further revealed that HIPK2 was ubiquitylated by Smurf2 (*Figure S5C*). Collectively, Smurf2 was transcriptionally activated by ATF4, which led to ubiquitination and degradation of HIPK2.

Activating transcription factor 4 contributes to high glucose-induced cardiac fibrosis and oxidative stress via up-regulating Smad ubiquitin regulatory factor 2

To verify the involvement of Smurf2 in ATF4-mediated diabetic cardiac fibrosis, ATF4-silenced HL-2 cells were further transfected with oeSmurf2. The expression level of Smurf2 was raised by HG stimulation. ATF4 inhibition remarkably reduced Smurf2 expression in HG-exposed cells, which was abolished by Smurf2 overexpression (*Figure 6A,B*). Additionally, ATF4 knockdown-induced promotion in cell viability and inhibition in apoptosis of HG-challenged cells could be attenuated by Smurf2 overexpression (*Figure 6C,D*). Moreover, the declined SOD and GSH-Px activities, and raised MDA and ROS levels in response to HG were counteracted after ATF4 was silenced alone, which were abrogated by co-transfection with oeSmurf2 (*Figure 6E–G*; *Figure S6A*). Accordingly, ATF4 depletion-mediated down-regulation of collagen I and collagen III, and up-regulation of HIPK2, nuclear Nrf2 and HO-1 in HG-challenged cells was partly reversed by Smurf2 overexpression (*Figure S6B*). The above observations suggested that ATF4/Smurf2 axis facilitated HG-induced cardiac fibrosis and oxidative stress.

Discussion

DC has caused extensive concern due to the unsatisfactory efficacy of conventional therapy for heart failure and blood glucose control, which remains a troublesome problem in clinic.[22,23] Currently, the detailed molecular mechanisms underlying the pathological progression of DC have not been clarified. In this work, the regulatory role of ATF4 in DC and its potential mechanisms were explored. Our data showed that ATF4 was up-regulated in the hearts of diabetic mice and HG-exposed cardiomyocytes. Silencing of ATF4 repressed fibrosis and oxidative stress to protect against DC *in vivo* and *in vitro*. Mechanistically, ATF4 transcriptionally activated Smurf2 to facilitate ubiquitination and degradation of HIPK2, thereby inactivating Nrf2/HO-1 pathway. Our findings provide novel insights into the pathological mechanisms of DC, and suggest that targeting ATF4 may be an effective intervention for DC.

It has been recognized that heart functional impairment in DC is due to myocardial pathological structure, featured by excessive collagen deposition.[24] Cardiac fibrosis caused by collagen fibre formation may result in stiffness of the myocardium and affect myocardial function.[25] In line with previous study, we found that fibrosis and collagen were deposited in the hearts of diabetic mice and HG-challenged cardiomyocytes. Notably, ATF4 was up-regulated in the *in vivo* and *in vitro* models of DC. ATF4 is a multifunctional transcription regulatory protein that is involved in a wide range of pathophysiological processes, such as apoptosis,[26] angiogenesis,[27] oxidative stress,[28] tumourigenesis,[29] and so on. ATF4 has been documented to contribute to fibrosis of various organs. Liang et al. reported that ATF4 facilitated renal tubulointerstitial fibrosis during the progression of diabetic nephropathy.[10] Besides, ATF4 activation could accelerate the development of hepatic fibrosis.[30] Previous studies have reported that ATF4 played pivotal roles in skeletal muscle atrophy.[10,31] This study mainly focused on the influence of ATF4 on cardiac fibrosis. We found that ATF4 silencing effectively improved cardiac function as confirmed by elevating LVEF and LVFS, restrained cardiac fibrosis via decreasing collagen I and III expression. These results suggested that ATF4 promoted diabetes-induced cardiac fibrosis by enhancing collagen fibre formation. However, the other potential effects of ATF4 in diabetic mice need to be explored in the future.

Oxidative stress, the result of excessive ROS production, is a key feature of DC.[32] Inhibition of ROS production is considered to inhibit the development of DC.[33] Additionally, in response to ROS stimulation, the activities of antioxidative enzymes SOD and GSH-Px can be reduced, but the level of MDA, a product of lipid peroxidation, can be raised.[34] In our study, knockdown of ATF4 attenuated ROS and MDA overproduction, and enhanced SOD and GSH-Px activities *in vivo* and *in vitro*. The viability of myocardial cells determines the cardiac contractility, and therefore apoptosis of cardiomyocytes attributed to oxidative stress injury may lead to cardiac dysfunction.[23] Suppression of ATF4 has been revealed to protect cardiomyocytes from apoptosis.[35] In accordance with the previous study, we found that ATF4 silencing raised cell viability and restrained apoptosis of HG-stimulated cardiomyocytes. Thus, ATF4 inhibition alleviated DC via suppressing oxidative damage and apoptosis.

Although the biological function of ATF4 in cardiac fibrosis, oxidative stress and apoptosis has been explored, the downstream mechanisms of ATF4 remain unclear. Smurf2, an E3 ubiquitin ligase, has been identified as a pivotal modulator of DC, due to its regulation in ubiquitin proteasome

Figure 6 Smurf2 is involved in ATF4-induced cardiac fibrosis and oxidative stress in HG-stimulated cardiomyocytes. (A, B) The mRNA and protein levels of Smurf2 in HL-1 cells were determined by RT-qPCR and western blotting. (C) MTT assay was adopted to detect cell viability. (D) Apoptotic rate of HL-1 cells was measured by flow cytometry. (E) SOD activity, (F) GSH-Px activity, (G) MDA level in HL-1 cells were assessed. Data are presented as the mean ± SD (n = 3). *$P < 0.05$, **$P < 0.01$, ***$P < 0.001$.

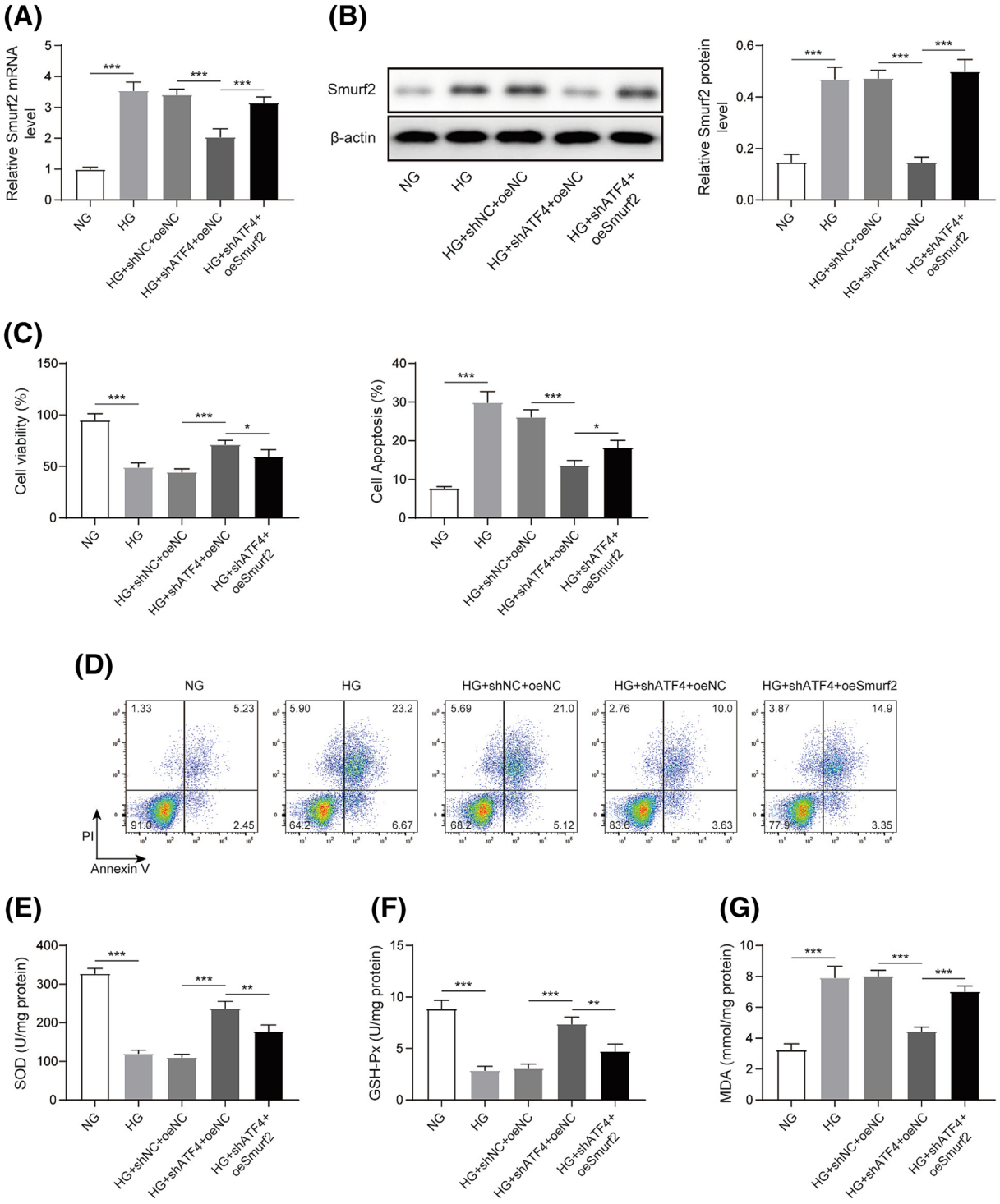

DOI: 10.1002/ehf2.14404

degradation.[12] Moreover, Smurf2 has been validated as a novel target for cardiac fibrosis via the regulation of TGF-β signalling.[36] In the current study, Smurf2 was down-regulated by ATF4 silencing. Furthermore, we validated a direct interaction between ATF4 and Smurf2. HIPK2, as a nuclear serine/threonine kinase, plays crucial roles in the promotion of tumour cell apoptosis.[37] Under hypoxia condition, HIPK2 can be degraded by E3 ubiquitin ligases during cancer progression.[38] A previous study indicated that HIPK2 protein degradation could be triggered by hyperglycaemia.[39] Dang et al. demonstrated that HIPK2 overexpression protected cardiomyocytes against hypoxia/reoxygenation injury through activating Nrf2/HO-1 pathway.[20] Mounting evidence has proved that activation of Nrf2/HO-1 pathway exhibited protective effects on DC.[15,40] Interestingly, our findings demonstrated that HIPK2 could interact with Smurf2. Depletion of Smurf2 suppressed the ubiquitination and degradation of HIPK2, thus promoting HIPK2 expression in myocardial cells. Additionally, ATF4 knockdown-mediated protection against cardiomyocyte fibrosis, oxidative stress, and apoptosis, and Nrf2/HO-1 pathway activation could be abolished by Smurf2 overexpression. Taken together, these results suggested that ATF4 silencing exerted beneficial effects on DC through inhibiting Smurf2-mediated ubiquitination and degradation of HIPK2, and subsequent activation of Nrf2/HO-1 pathway.

In conclusion, our findings uncovered a novel pathological mechanism of DC through which ATF4 contributed to cardiac fibrosis and dysfunction. Knockdown of ATF4 activated Nrf2/HO-1 pathway via repressing Smurf2-mediated ubiquitination and degradation of HIPK2, which relieved DC by inhibiting fibrosis, oxidative damage, and apoptosis. Targeting ATF4 may be an effective treatment for DC.

Funding

None.

Conflict of interest

The authors declare that they have no conflict of interest.

Supporting information

Additional supporting information may be found online in the Supporting Information section at the end of the article.

Figure S1. Basic characteristics and cardiac functional parameters of mice. (A) Body weight, (B) heart weight, (C) fasting blood glucose concentration, (D) fasting blood insulin level of mice were detected. (E) diastolic and systolic LVPW, (F) diastolic and systolic LVAW, (G) LVSD, (H) LVDD, (I) LVSV, (J) LVDV were detected by M-mode echocardiography. Data are presented as the mean ± SD (n = 5). $*P < 0.05$, $**P < 0.01$.

Figure S2. ATF4 knockdown attenuates cardiac fibrosis in myocardial infarction (MI) mice. (A) The mRNA level of ATF4 in heart tissues was measured by RT-qPCR. (B) RT-qPCR analysis of Collagen I and Collagen III mRNA abundance in heart tissues. Data are presented as the mean ± SD (n = 5). $*P < 0.05$, $**P < 0.01$, $***P < 0.001$.

Figure S3. Western blotting analysis of Collagen I, Collagen III, ATF4, HIPK2, nuclear Nrf2 and HO-1 protein expression in HL-1 cells. Data are presented as the mean ± SD (n = 3). $***P < 0.001$.

Figure S4. Western blotting was performed to detect Collagen I, Collagen III, HIPK2, nuclear Nrf2 and HO-1 protein expression in HL-1 cells. Data are presented as the mean ± SD (n = 3). $***P < 0.001$.

Figure S5. (A) HIPK2 degradation in response to CHX was measured. (B) Effect of Smurf2 knockdown on HIPK2 degradation was determined. (C) Smurf2-mediated ubiquitination of HIPK2 was confirmed by co-IP assay. Data are presented as the mean ± SD (n = 3). $*P < 0.05$, $**P < 0.01$.

Figure S6. (A) ROS level in HL-1 cells was detected by DCFH-DA staining. (B) Western blotting analysis for detection of Collagen I, Collagen III, HIPK2, nuclear Nrf2 and HO-1 protein expression in HL-1 cells. Data are presented as the mean ± SD (n = 3). $***P < 0.001$.

Figure S7. Supporting information.

Table S1. Oligonucleotide primer sets for qPCR.

References

1. Dillmann WH. Diabetic cardiomyopathy. *Circ Res*. 2019; **124**: 1160–1162.
2. Tuleta I, Frangogiannis NG. Fibrosis of the diabetic heart: clinical significance, molecular mechanisms, and therapeutic opportunities. *Adv Drug Deliv Rev*. 2021; **176**: 113904.
3. Joshi M, Kotha SR, Malireddy S, Selvaraju V, Satoskar AR, Palesty A, McFadden DW, Parinandi NL, Maulik N. Conundrum of pathogenesis of diabetic cardiomyopathy: role of vascular endothelial dysfunction, reactive oxygen species, and mitochondria. *Mol Cell Biochem*. 2014; **386**: 233–249.
4. Ameri K, Harris AL. Activating transcription factor 4. *Int J Biochem Cell Biol*. 2008; **40**: 14–21.
5. Luo B, Lin Y, Jiang S, Huang L, Yao H, Zhuang Q, Zhao R, Liu H, He C, Lin Z. Endoplasmic reticulum stress eIF2α-ATF4 pathway-mediated cyclooxygenase-2 induction regulates cadmium-induced autophagy in kidney. *Cell Death Dis*. 2016; **7**: e2251.
6. Siwecka N, Rozpedek W, Pytel D, Wawrzynkiewicz A, Dziki A, Dziki L,

Diehl JA, Majsterek I. Dual role of endoplasmic reticulum stress-mediated unfolded protein response signaling pathway in carcinogenesis. *Int J Mol Sci*. 2019; **20**: 4354.
7. Kiesel VA, Sheeley MP, Hicks EM, Andolino C, Donkin SS, Wendt MK, Hursting SD, Teegarden D. Hypoxia-mediated ATF4 induction promotes survival in detached conditions in metastatic murine mammary cancer cells. *Front Oncol*. 2022; **12**: 767479.
8. Sobajima M, Miyake M, Hamada Y, Tsugawa K, Oyadomari M, Inoue R, Shirakawa J, Arima H, Oyadomari S. The multifaceted role of ATF4 in regulating glucose-stimulated insulin secretion. *Biochem Biophys Res Commun*. 2022; **611**: 165–171.
9. Cong XQ, Piao MH, Li Y, Xie L, Liu Y. Bis (maltolato)oxovanadium (IV) (BMOV) attenuates apoptosis in high glucose-treated cardiac cells and diabetic rat hearts by regulating the unfolded protein responses (UPRs). *Biol Trace Elem Res*. 2016; **173**: 390–398.
10. Liang Q, Liu T, Guo T, Tao W, Chen X, Chen W, Chen L, Xiao Y. ATF4 promotes renal tubulointerstitial fibrosis by suppressing autophagy in diabetic nephropathy. *Life Sci*. 2021; **264**: 118686.
11. Koganti P, Levy-Cohen G, Blank M. Smurfs in protein homeostasis, signaling, and cancer. *Front Oncol*. 2018; **8**: 295.
12. Dong L, Li JC, Hu ZJ, Huang XR, Wang L, Wang HL, Ma RCW, Lan HY, Yang SJ. Deletion of Smad3 protects against diabetic myocardiopathy in db/db mice. *J Cell Mol Med*. 2021; **25**: 4860–4869.
13. Yuan H, Xu J, Zhu Y, Li L, Wang Q, Yu Y, Zhou B, Liu Y, Xu X, Wang Z. Activation of calcium sensing receptor mediated autophagy in high glucose induced cardiac fibrosis in vitro. *Mol Med Rep*. 2020; **22**: 2021–2031.
14. Raish M, Ahmad A, Bin Jardan YA, Shahid M, Alkharfy KM, Ahad A, Ansari MA, Abdelrahman IA, al-Jenoobi FI. Sinapic acid ameliorates cardiac dysfunction and cardiomyopathy by modulating NF-kappaB and Nrf2/HO-1 signaling pathways in streptozocin induced diabetic rats. *Biomed Pharmacother*. 2021; **145**: 112412.
15. Li H, Shi Y, Wang X, Li P, Zhang S, Wu T, Yan Y, Zhan Y, Ren Y, Rong X, Xia T, Chu M, Wu R. Piceatannol alleviates inflammation and oxidative stress via modulation of the Nrf2/HO-1 and NF-κB pathways in diabetic cardiomyopathy. *Chem Biol Interact*. 2019; **310**: 108754.
16. Li Y, Duan JZ, He Q, Wang CQ. miR155 modulates high glucoseinduced cardiac fibrosis via the Nrf2/HO1 signaling pathway. *Mol Med Rep*. 2020; **22**: 4003–4016.
17. Xu L, Fang H, Xu D, Wang G. HIPK2 sustains inflammatory cytokine production by promoting endoplasmic reticulum stress in macrophages. *Exp Ther Med*. 2020; **20**: 171.
18. Zhou J, Li L, Hu H, Wu J, Chen H, Feng K, Ma L. Circ-HIPK2 accelerates cell apoptosis and autophagy in myocardial oxidative injury by sponging miR-485-5p and targeting ATG101. *J Cardiovasc Pharmacol*. 2020; **76**: 427–436.
19. Wang X, Zhang Z, Liang H, Chen R, Huang Y. Circ_0025908 regulates cell vitality and proliferation via miR-137/HIPK2 axis of rheumatic arthritis. *J Orthop Surg Res*. 2021; **16**: 472.
20. Dang X, Zhang R, Peng Z, Qin Y, Sun J, Niu Z, Pei H. HIPK2 overexpression relieves hypoxia/reoxygenation-induced apoptosis and oxidative damage of cardiomyocytes through enhancement of the Nrf2/ARE signaling pathway. *Chem Biol Interact*. 2020; **316**: 108922.
21. Marshall KD, Klutho PJ, Song L, Roy R, Krenz M, Baines CP. Cardiac myocyte-specific overexpression of FASTKD1 prevents ventricular rupture after myocardial infarction. *J Am Heart Assoc*. 2023; e025867.
22. Riehle C, Bauersachs J. Of mice and men: models and mechanisms of diabetic cardiomyopathy. *Basic Res Cardiol*. 2018; **114**: 2.
23. Jia G, Whaley-Connell A, Sowers JR. Diabetic cardiomyopathy: a hyperglycaemia- and insulin-resistance-induced heart disease. *Diabetologia*. 2018; **61**: 21–28.
24. Asbun J, Villarreal FJ. The pathogenesis of myocardial fibrosis in the setting of diabetic cardiomyopathy. *J Am Coll Cardiol*. 2006; **47**: 693–700.
25. Li L, Zhao Q, Kong W. Extracellular matrix remodeling and cardiac fibrosis. *Matrix Biol*. 2018; **68-69**: 490–506.
26. Li Y, She W, Guo T, Huang T, liu Y, Liu P, Xu X, Wang X, Wang M, Yu C, Liu Y, Wei Y. The organic arsenical-derived thioredoxin and glutathione system inhibitor ACZ2 induces apoptosis and autophagy in gastric cancer via ROS-dependent ER stress. *Biochem Pharmacol*. 2023; **208**: 115404.
27. Chen L, Liu X, Zhou H, Li G, Huang F, Zhang J, Xia T, Lei W, Zhao J, Li C, Chen M. Activating transcription factor 4 regulates angiogenesis under lipid overload via methionine adenosyltransferase 2A-mediated endothelial epigenetic alteration. *FASEB J*. 2021; **35**: e21612.
28. Wang X, Zhang G, Dasgupta S, Niewold EL, Li C, Li Q, Luo X, Tan L, Ferdous A, Lorenzi PL, Rothermel BA, Gillette TG, Adams CM, Scherer PE, Hill JA, Wang ZV. ATF4 protects the heart from failure by antagonizing oxidative stress. *Circ Res*. 2022; **131**: 91–105.
29. Guan L, Wang F, Wang M, Han S, Cui Z, Xi S, Xu H, Li S. Downregulation of HULC induces ferroptosis in hepatocellular carcinoma via targeting of the miR-3200-5p/ATF4 axis. *Oxid Med Cell Longev*. 2022; **2022**: 9613095–9613018.
30. Luo XH, Han B, Chen Q, Guo XT, Xie RJ, Yang T, Yang Q. Expression of PERK-eIF2alpha-ATF4 pathway signaling protein in the progression of hepatic fibrosis in rats. *Int J Clin Exp Pathol*. 2018; **11**: 3542–3550.
31. Ebert SM, Rasmussen BB, Judge AR, Judge SM, Larsson L, Wek RC, Anthony TG, Marcotte GR, Miller MJ, Yorek MA, Vella A, Volpi E, Stern JI, Strub MD, Ryan Z, Talley JJ, Adams CM. Biology of activating transcription factor 4 (ATF4) and its role in skeletal muscle atrophy. *J Nutr*. 2022; **152**: 926–938.
32. Ritchie RH, Abel ED. Basic mechanisms of diabetic heart disease. *Circ Res*. 2020; **126**: 1501–1525.
33. Doenst T, Nguyen TD, Abel ED. Cardiac metabolism in heart failure: implications beyond ATP production. *Circ Res*. 2013; **113**: 709–724.
34. Feng W, Lei T, Wang Y, Feng R, Yuan J, Shen X, Wu Y, Gao J, Ding W, Lu Z. GCN2 deficiency ameliorates cardiac dysfunction in diabetic mice by reducing lipotoxicity and oxidative stress. *Free Radic Biol Med*. 2019; **130**: 128–139.
35. Jeong MH, Jeong HJ, Ahn BY, Pyun JH, Kwon I, Cho H, Kang JS. PRMT1 suppresses ATF4-mediated endoplasmic reticulum response in cardiomyocytes. *Cell Death Dis*. 2019; **10**: 903.
36. Cunnington RH, Nazari M, Dixon IM. c-Ski, Smurf2, and Arkadia as regulators of TGF-beta signaling: new targets for managing myofibroblast function and cardiac fibrosis. *Can J Physiol Pharmacol*. 2009; **87**: 764–772.
37. D'Orazi G, Rinaldo C, Soddu S. Updates on HIPK2: a resourceful oncosuppressor for clearing cancer. *J Exp Clin Cancer Res*. 2012; **31**: 63.
38. Semenza GL. Defining the role of hypoxia-inducible factor 1 in cancer biology and therapeutics. *Oncogene*. 2010; **29**: 625–634.
39. Baldari S, Garufi A, Granato M, Cuomo L, Pistritto G, Cirone M, D'Orazi G. Hyperglycemia triggers HIPK2 protein degradation. *Oncotarget*. 2017; **8**: 1190–1203.
40. Li X, Wu D, Tian Y. Fibroblast growth factor 19 protects the heart from oxidative stress-induced diabetic cardiomyopathy via activation of AMPK/Nrf2/HO-1 pathway. *Biochem Biophys Res Commun*. 2018; **502**: 62–68.